Computational Materials Science 29 (2004) 459–474

COMPUTATIONAL MATERIALS SCIENCE

www.elsevier.com/locate/commatsci

A computational approach for prediction of the damage evolution and crushing behavior of chopped random fiber composites ☆

H.K. Lee [a,*], S. Simunović [b], D.K. Shin [c]

[a] Department of Civil, Architectural, and Environmental Engineering, University of Miami, Coral Gables, FL 33124-0620, USA
[b] Computer Science and Mathematics Division, Oak Ridge National Laboratory, Oak Ridge, TN 37831-6359, USA
[c] Department of Civil Engineering, Myongji University, Yongin 449-728, South Korea

Received 20 August 2003; received in revised form 3 November 2003; accepted 9 December 2003

Abstract

A computational model is developed, by implementing the damage models previously proposed by authors into a finite element code, for simulating the damage evolution and crushing behavior of chopped random fiber composites. Material damages induced by fiber debonding and crack nucleation and growth are considered. Systematic computational algorithms are developed to combine the damage models into the constitutive relation. Based on the implemented computational model, a range of simulations are carried out to probe the behavior of the composites and to validate the proposed methodology. Numerical examples show that the present computational model is capable of modeling progressive deterioration of effective stiffness and softening behavior after the peak load. Crushing behavior of composite tube is also simulated, which shows the applicability of the proposed computational model for crashworthiness simulations.

Keywords: Damage evolution; Crushing behavior; Finite element implementation; Chopped random fiber composites; Crashworthiness simulations

1. Introduction

Chopped random fiber composites are being used increasingly as structural components in aerospace, infrastructure and automotive applications, due to rapid advances in processing science and engineering. These materials have desirable engineering properties (e.g., high strength and stiffness, low density, and high damage tolerance) and can be tailored to meet the intended function of the component. In brittle composites such as

☆ The submitted manuscript has been authored by a contractor of the US Government under contract No. DE-AC05-00OR22725. Accordingly, the US Government retains a non-exclusive, royalty-free license to publish or reproduce the published form of this contribution, or allow others to do so, for US Government purposes.

* Corresponding author. Tel.: +1-305-284-3457; fax: +1-305-284-3492.

E-mail address: hlee@miami.edu (H.K. Lee).

0927-0256/$ - see front matter © 2004 Elsevier B.V. All rights reserved.
doi:10.1016/j.commatsci.2003.12.008

quasi-brittle chopped random fiber composites and concrete, the interfacial microcracks by the debonding of inclusions and the matrix usually form first due to the fact that (1) the size of interfacial cracks is usually much larger than that of the matrix voids or cracks and (2) the interfacial layer (transition zone) has a poor microstructure that results in a weaker fracture toughness [22].

Several attempts have been made to accurately model the fiber/matrix interfacial damage. Duva et al. [34] combined an interfacial constitutive model and a probabilistic model to yield an approach for modeling the stress–strain response of fibrous composites with fiber/matrix interfacial damage. Wu et al. [31] performed an axisymmetric variational analysis of stress transfer into fibers through a partially debonded interface. They treated the debonded interface as an external boundary on which a presumed interfacial shear stress was specified. Zhao and Weng [32,33] and Ju and Lee [13] assumed that a partially debonded fiber can be replaced by an equivalent, perfectly bonded fiber that possesses yet unknown transversely isotropic moduli. In their study, the transverse isotropy of the equivalent fiber was determined based on the assumption that its tensile and shear stresses always vanish in the debonded direction, and its stress components in the bonded directions exist. Most recently, Meddad et al. [21] developed a simple micromechanical constitutive model based on the Carman and Reifsnider approach [7] for short fiber reinforced composites undergoing debonding damage.

Although the damage for quasi-brittle chopped random fiber composites is governed by a combined mechanisms, such as interfacial debonding between fibers and the matrix and the subsequent crack nucleation and growth, one damage mechanism is dominant compared to the others depending upon the level of load or deformation. At a smaller load level far below the peak stress in the stress–strain curve, the interfacial debonding usually dominates the damage behavior. As the load increases up to the peak load, the subsequent nucleation of microcracks dominates and major cracks will form from the coalescence of microcracks near the peak load. As the number of cracks multiplies and crack-driving force exceeds the fracture toughness of the materials near the peak load, the balance tilts from the crack nucleation to crack growth [16]. For example, Karihaloo and Huang [15] assumed in their study of damage model for quasi-brittle materials that the stable propagation of microcracks continues until the peak load is reached. Since the microcracks are isolatedly and randomly distributed during this stage, the prepeak nonlinear stress and strain response may be described by using a scalar damage mechanics approach. A macroflaw will form from coalescence of microcracks as the load increases. The major crack will propagate unstably after the peak stress and as a result a softening type of stress–strain curve will be observed.

Several models have been proposed to describe the intrinsic softening of quasi-brittle materials. Most of the models introduced by Horii et al. [12], Ortiz [25], and Karihaloo et al. [14] are based on the assumption that unbroken ligaments bridge across a discontinuous macroflaw. Sirivedin et al. [29] used linear elastic and elasto-plastic finite element analyses to investigate the initiation and propagation of a matrix crack in short-carbon fiber/epoxy composites. A maximum hoop-strain criterion and the modified Rice and Tracey microvoid nucleation, growth, and coalescence model were used in their derivation. Most recently, Lee and Simunovic [18,19], Lee [17], and Lee and Simunovic [20] have presented damage constitutive models based on micromechanics and continuum damage mechanics to predict the overall response and damage evolution in aligned and chopped random fiber composites. A more detailed review of damage in chopped random fiber composites can be found in [23,24,4,29].

Predictive analytical and numerical tools required to accurately evaluate and design structural components made of chopped random fiber composites do not currently exist. The availability of predictive tools will be extremely helpful in decreasing the design process time and cost by reducing component testing and increasing the simulation accuracy of chopped random fiber composite structures. A numerical program of research is conducted to develop computational model, by implementing the damage models previously proposed by authors into a finite element code, for simulating the damage evolution and crushing behavior of chopped random fiber composites. Material damages induced by the interfacial fiber debonding, and nucleation and growth of microcracks are considered. Debonding on the interface between fibers and the matrix is simulated by using the micromechanical damage model [17–19] and the subsequent crack nucleation and growth in the matrix is treated in the framework of the continuum fracture mechanics [20].

The composites are assumed to be brittle and to have isotropic microcrack distribution. It is also assumed that the damage evolution in the composites is gradual and proportional. By using user-supplied material subroutine, the micromechanics and continuum damage mechanics-based damage models are incorporated into the nonlinear finite element code DYNA3D. The overall properties of microcracked composites are estimated using the differential scheme. Using the developed computational algorithm, numerical simulations for a composite plate coupon test and for an automotive structural component under crash load are carried out to probe damage evolution and crushing behavior of the composites. The proposed damage models are related to model parameters that have to be determined. A comprehensive program involving laboratory experiments and numerical simulations will be needed to determine the model parameters for the calibration of the constitutive model.

2. Damage models

2.1. Introduction

Let us consider a composite consisting of an elastic matrix (phase 0), randomly oriented perfectly bonded fibers (phase 1), penny-shaped cracks (phase 2), and partially debonded fibers (phase 3). It is assumed that the damaged state can be described by the volume fraction of partially debonded fibers ϕ_3, number of microcracks in unit volume N and the average size $\bar{c}$ of microcracks.

The effects of interactions among constituents, including the fiber–crack interaction, on the overall behavior of composites with moderate and high concentration of reinforcements will be significant once the deductive approach based on micromechanical analysis is used. However, the proposed damage model is pheonomenological. It combined concepts from fracture mechanics and Eshelby's inclusion theory to describe complexity of the damage constitutive responses, and used analogies that are physical in their nature. Hence, the interactions among constituents are not essential in the current pheonomenological damage model.

Systematic computational algorithms will be developed to combine the damage models into the constitutive relation. The computational algorithms consist of three computational phases denoted by ID, CN and CG. The ID phase is related to the Eshelby's inclusion theory for interfacial debonding between fibers and matrix, while the CN and CG phases are associated with the fracture mechanics-based model for crack nucleation and growth, respectively. The debonding of fibers is assumed to be controlled by the stress of the fibers and the statistical behavior of the fiber–matrix interfacial strength in the form of Weibull probability density function. The formulation of the stress of the fibers needed to initiate the fiber debonding was explicitly derived by Ju and Lee [13] and Lee and Simunovic [19], where the Eshelby's inclusion theory and an orientational average process were employed to derive the stresses of the fibers. The employed orientational average process for 3-D random case [18] is identical to that of Tandon and Weng [30].

Since the Eshelby's inclusion theory is based on infinitesimal deformation framework, the ID phase is restricted to small strain range. However, after the ID phase, cracks start to nucleate (CN phase) and grow (CG phase) into adjacent medium based on the fracture mechanics. CN and CG phases therefore allow for large deformation. In the model derivation, rate-dependency is present and is modeled in crack nucleation and growth phases.

2.2. Probabilistic micromechanics: interfacial debonding between fibers and the matrix

A micromechanics damage constitutive model proposed by Lee and Simunovic [18,19] and

Lee [17] for randomly oriented discontinuous fiber-reinforced composites is employed to model interfacial debonding between fibers and the matrix. In this micromechanics-based damage model, progressive interfacial debonding between fibers and the matrix is assumed to be controlled by the stress of the fibers and the statistical behavior of the fiber–matrix interfacial strength in the form of Weibull probability density function. Only a brief outline of the model is presented in this paper and detail descriptions of the model can be found in [17].

The volume fraction of the partially debonded fibers ϕ_3 can be derived, by applying the Weibull's statistical function

$$p[(\bar{\sigma}_{\mathrm{f}})_{\mathrm{m}}] = \left(\frac{S_0}{M}\right)\left[\frac{(\bar{\sigma}_{\mathrm{f}})_{\mathrm{m}}}{S_0}\right]^{M-1} \cdot \exp\left\{-\left[\frac{(\bar{\sigma}_{\mathrm{f}})_{\mathrm{m}}}{S_0}\right]^{M}\right\} \tag{1}$$

where the hydrostatic tensile stresses of the fibers $(\bar{\sigma}_{\mathrm{f}})_{\mathrm{m}} = [(\bar{\sigma}_{11})_{\mathrm{f}} + (\bar{\sigma}_{22})_{\mathrm{f}} + (\bar{\sigma}_{33})_{\mathrm{f}}]/3$. The formulation of the stress of the fibers needed to initiate the fiber debonding was explicitly derived by Ju and Lee [13] and Lee and Simunovic [19], where the Eshelby's inclusion theory and an orientational average process were employed to derive the stresses of the fibers. The employed orientational average process for 3-D random case [18] is identical to that of Tandon and Weng [30]. The constants S_0 and M in Eq. (1) are scale (Weibull modulus) and shape parameters of the Weibull function, respectively. The methods determining values of these parameters are introduced in [8,17].

Using the Weibull function in Eq. (1), the current partially debonded (damaged) fiber volume fraction ϕ_3 at a given level of $(\bar{\sigma}_{\mathrm{f}})_{\mathrm{m}}$ can be obtained as

$$\begin{aligned}\phi_3 &= \phi \cdot P_d[(\bar{\sigma}_{\mathrm{f}})_{\mathrm{m}}] \\ &= \phi \cdot \left\{1 - \exp\left[-\left(\frac{(\bar{\sigma}_{\mathrm{f}})_{\mathrm{m}}}{S_0}\right)^{M}\right]\right\}\end{aligned} \tag{2}$$

where ϕ is the original fiber volume fraction.

2.3. Continuum fracture mechanics-based damage model: crack nucleation and growth

The following model derivation is identical to the model in [20] and is here repeated for completeness of the proposed numerical model.

The model derivation in this section is identical to the model by Lee and Simunovic [20] and is here repeated for completeness of the proposed numerical model. The basic assumption of the fracture mechanics-based damage model is that the damaged state of a solid can be described by the number of microcracks per unit volume N and the average size $\bar{c}$ of microcracks. The constitutive relation for the composites with microcracks distributed in a statistically uniform manner can be expressed as

$$\boldsymbol{\sigma} = \mathbf{C}(\bar{c}, N) : \boldsymbol{\epsilon} \tag{3}$$

where ":" denotes the tensor contraction, $\boldsymbol{\sigma}$ is the macroscopic stress, $\mathbf{C}$ is the overall stiffness tensor, $\boldsymbol{\epsilon}$ is the macroscopic strain. The rate form of Eq. (3) can be expressed as

$$\dot{\boldsymbol{\sigma}} = \frac{\partial \mathbf{C}}{\partial N}\dot{N} : \boldsymbol{\epsilon} + \frac{\partial \mathbf{C}}{\partial \bar{c}}\dot{\bar{c}} : \boldsymbol{\epsilon} + \mathbf{C} : \dot{\boldsymbol{\epsilon}} \tag{4}$$

The above material model is therefore fully defined by the crack growth rate $\dot{\bar{c}}$, crack nucleation rate $\dot{N}$, and their respective effect on the overall stiffness tensor. The rate form of the constitutive relation in Eq. (4) can be solved by applying numerical integration. As mentioned in Section 1, it is assumed that the damage is proportional. The equivalent incremental form for the Eq. (4) can be written as

$$\begin{aligned}\boldsymbol{\sigma}_{n+1} = \boldsymbol{\sigma}_n &+ \mathbf{C} : \Delta\boldsymbol{\epsilon}_{n+1} + \frac{\partial \mathbf{C}}{\partial \bar{c}}\Delta\bar{c}_{n+1} : \boldsymbol{\epsilon}_n \\ &+ \frac{\partial \mathbf{C}}{\partial \bar{c}}\Delta\bar{c}_{n+1} : \Delta\boldsymbol{\epsilon}_{n+1} + \frac{\partial \mathbf{C}}{\partial N}\Delta N_{n+1} : \boldsymbol{\epsilon}_n \\ &+ \frac{\partial \mathbf{C}}{\partial N}\Delta N_{n+1} : \Delta\boldsymbol{\epsilon}_{n+1}\end{aligned} \tag{5}$$

where the subscript n denotes the nth integration time step.

2.3.1. Rate of crack nucleation

Previous investigations on the nucleation of microcracks for several materials [5,26,28, 9,27] have shown that the nucleation rate $\dot{N}$ of microcracks can be expressed as exponential relations, under the applied stress σ:

$$\dot{N} = \dot{N}_0 \cdot \exp\left[\frac{\sigma - \sigma_{n0}}{\sigma_1}\right], \quad \sigma > \sigma_{n0}$$
$$= 0, \quad \sigma < \sigma_{n0} \tag{6}$$

where σ_{n0} is the threshold stress for the nucleation of microcracks, and $\dot{N}_0$ and σ_1 are experimentally determined material parameters. It is assumed that the applied stress $\sigma = [(\sigma_{11}) + (\sigma_{22}) + (\sigma_{33})]/3$. It is worth mentioning that the rate equation for crack nucleation in Eq. (6) is applicable to both ductile and brittle materials [27]. More complex forms have been also used in the literature and can be substituted for Eq. (6) (e.g., [2]).

In the model derivation, the composites are assumed to be brittle, and the size of crack does not correspond directly to the actual crack size but is the concept to model progressive damage observed in the experiments on the macroscopic level. Also the failure strain of composite specimens used in drop tower test was less than 1% (extremely brittle). Therefore, the rate equation for crack nucleation in Eq. (6) could be employed for modeling the crack nucleation in brittle chopped random fiber composites.

The incremental form for numerical approximation of Eq. (6) by the backward Euler integration scheme can be written as

$$N_{n+1} = N_n + \Delta t_{n+1}\dot{N}_0 \cdot \exp\left[\frac{(\sigma)_{n+1} - \sigma_{n0}}{\sigma_1}\right] \tag{7}$$

In this study, the incremental nonlinear equation for the crack nucleation N is solved using the Newton's method.

2.3.2. Crack growth criteria

The crack growth criteria proposed by Addessio and Johnson [1] is employed. In their paper, the instability criteria for a single crack was derived by considering the energy balance around the microcrack. Applying the volume averaging procedure with the assumptions of an exponential crack size distribution and isotropy, the damage surfaces for a continuum with microcracks are obtained in terms of the pressure p and the deviatoric stress q defined as

$$p = -\frac{1}{3}\sigma_{ii}, \quad q = \sqrt{\frac{3}{2}q_{ij}q_{ij}} \tag{8}$$

where $q_{ij} = \sigma_{ij} + p\delta_{ij}$.

The damage surface in case of tension ($p < 0$) is (see Addessio and Johnson [1])

$$F^n(p, q, \bar{c}) = q^2 + \frac{45}{4(5 - v_0)}\left[(2 - v_0)p^2 - \frac{2K}{\bar{c}}\right] = 0 \tag{9}$$

In compression ($p > 0$) (see Addessio and Johnson [1]),

$$F^t(p,q,\bar{c}) = q^2 - \frac{45}{2(3-2v_0^2)} \times \left[(\mu_{\mathrm{fr}}p + \sigma_0)\left(\mu_{\mathrm{fr}}p + \sigma_0 + \sqrt{\frac{\pi K}{\bar{c}}}\right) + \frac{K}{\bar{c}}\right] = 0 \tag{10}$$

In the above expression, σ_0 is the cohesive stress, μ_{fr} is the coefficient of friction, and K is defined as

$$K \equiv \frac{\pi}{2}\frac{2 - v_0}{1 - v_0}K_{\mathrm{IC}}G_0 \tag{11}$$

where K_{IC} is the plane strain fracture toughness of the brittle solids.

2.3.3. Rate of crack growth

Cracks grow at a fraction of Rayleigh wave speed which for applications is approximated by the shear wave velocity [1]. The rate of crack growth can be expressed as (see Addessio and Johnson [1])

$$\dot{\bar{c}} = \beta\dot{c}_{\max}\tanh(d_{\mathrm{s}}) \tag{12}$$

where $\dot{c}_{\max}$ is the shear wave speed $\left(\dot{c}_{\max} = \sqrt{\frac{E^*}{\rho^*}}\right)$, in which E^* and ρ^* are the overall Young's modulus and the density, respectively, of the material, d_{s} is the measure of the distance the amount by which the state of stress exceeds the damage surface, and β is a scaling factor for crack speed and is assumed to be a constant. It should be noted that Eq. (12) is a rate-dependent approach to determine crack growth rate $\dot{\bar{c}}$ and it implies that the final stress lies above the damage surface [1].

The rate equation in Eq. (12) can be solved by applying a standard numerical integration technique. For the backward Euler method, the rate equation can be written in an incremental form as

$$\bar{c}_{n+1} = \bar{c}_n + \beta\Delta t_{n+1}\sqrt{\frac{(E^*)_{n+1}}{(\rho^*)_{n+1}}}\tanh(d_\mathrm{s}) \tag{13}$$

where $\bar{c}_{n+1}$ denotes the size of microcrack at time $t = t_{n+1}$.

The stresses calculated for a specified velocity field, or equivalently, the strain rate, the state of stress can be used to determine the stability of the crack using the criteria expressed in Eqs. (9) and (10). If the stress state is within the damage surface, then the deformation is elastic and there are no changes in the mean crack size. If, however, the stress state is outside the damage surface, then the changes in the mean crack size are obtained from Eq. (12).

2.4. Effective moduli of microcracked solids

In this study, the differential scheme derived by Hashin [11] is employed to obtain the effective elastic moduli of microcracked composites. The normalized elastic moduli of a solid containing randomly distributed penny-shaped cracks can be summarized as

$$\frac{E^*}{E_0} = \left(\frac{\nu^*}{\nu_0}\right)^{10/9}\left(\frac{3-\nu_0}{3-\nu^*}\right)^{1/9} \tag{14}$$

$$\frac{G^*}{G_0} = \frac{1+\nu_0}{1+\nu^*}\frac{E^*}{E_0} \tag{15}$$

$$\omega = \frac{5}{8}\ln\frac{\nu_0}{\nu^*} + \frac{15}{64}\ln\frac{1-\nu^*}{1-\nu_0} + \frac{45}{128}\ln\frac{1+\nu^*}{1+\nu_0} + \frac{5}{128}\ln\frac{3-\nu^*}{3-\nu_0} \tag{16}$$

where ν_0, E_0, G_0 are the Poisson's ratio, Young's modulus, and shear modulus, respectively, of uncracked solid; and ν^*, E^*, G^* are the effective Poisson's ratio, Young's modulus, and shear modulus, respectively, of a cracked solid. $\omega = N\bar{c}^3$, in which N is the number of cracks in composites and $\bar{c}$ is the mean crack radius, signifies the crack density parameter. The Newton iteration method is utilized to obtain the normalized elastic moduli E^*/E_0, G^*/G_0, and ν^*/ν_0.

3. Numerical algorithms for progressive damage modeling

The micromechanics and fracture mechanics-based damage models are implemented into the explicit finite element code DYNA3D. By writing the subroutines for user supplied materials and incorporating them into the nonlinear finite element program, the progressive damage evolutions due to the interfacial fiber debonding, nucleation of microcracks, and growth of microcracks are taken into account into the constitutive relation for the chopped random fiber composites. The finite element implementation allows us to analyze various numerical tests, to simplify investigation of the effects of modeling variables, and to perform customized post-processing of the data that would be most applicable for this study.

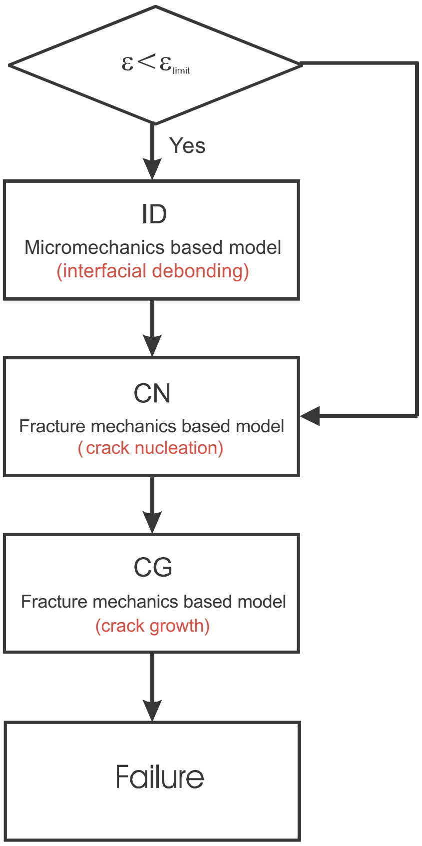

Fig. 1. Overall algorithm for user-supplied subroutine.

The overall scheme for the user-supplied material subroutines simulating the progressive damage behavior of composite materials for a specified loading or displacement is shown in Fig. 1. The algorithm consists of three computational phases denoted by ID, CN, and CG. The ID phase, which is restricted to small strain range ($\epsilon \leqslant \epsilon_{\text{limit}}$; e.g., $\epsilon_{\text{limit}} = 0.01, 0.015$), is related to the micromechanics-based damage model for interfacial debonding between fibers and the matrix, and the CN and CG phases are associated with the fracture mechanics-based model for crack nucleation and crack growth phases, respectively. The input parameters for the user subroutine consist of the material properties E_{m}, v_{m}, E_{f}, v_{f}; the volume fraction and aspect ratio of fibers ϕ, α; the Weibull parameters S_0, M; the crack nucleation related parameters $\dot{N}_0$, σ_{n0}, σ_1; and the crack growth related parameters $\bar{c}_0$, N_0, μ_{fr}, β. In the user-material subroutines, history variables, such as the volume fraction of damaged fibers, the number of microcracks, and the mean crack size, are updated at each time increment step.

Fig. 2(a)–(c) show detailed computational procedures for ID, CN, and CG phases, respectively.

(a)

(a) Initialize : set $z = 0$; $(\phi_1)_{n+1}^{(0)} = (\phi_1)_n,\ (\phi_2)_{n+1}^{(0)} = (\phi_2)_n$

(b) Compute :

Effective moduli : $(E^*)_{n+1}^{(z)},\ (\nu^*)_{n+1}^{(z)}$;

Internal stresses of fibers : $[(\bar{\sigma}_m)_1]_{n+1}^{(z)}$

(c) Compute the Weibull probability distribution function :

$$P_d\left\{[(\bar{\sigma}_m)_1]_{n+1}^{(z)}\right\} = 1 - exp\left[-\left(\frac{[(\bar{\sigma}_m)_1]_{n+1}^{(z)}}{S_o}\right)^M\right]$$

(d) Compute volume fractions :

$$(\phi_2)_{n+1}^{(z)} = \phi \cdot P_d\{[(\bar{\sigma}_m)_1]_{n+1}^{(z)}\} = \phi \cdot \left\{1 - exp\left[-\left(\frac{[(\bar{\sigma}_m)_1]_{n+1}^{(z)}}{S_o}\right)^M\right]\right\},$$

$$(\phi_1)_{n+1}^{(z)} = \phi - (\phi_2)_{n+1}^{(z)}$$

(e) Perform convergence check :

If $\left|\dfrac{(\phi_1)_{n+1}^{(z)} - (\phi_1)_{n+1}^{(z-1)}}{(\phi_1)_{n+1}^{(z-1)}}\right| \leq Tol\ \ (e.g.,\ 10^{-8})$: then update quantities in (b), (c), (d)

$$(E^*)_{n+1} = (E^*)_{n+1}^{(z)},\ (\nu^*)_{n+1} = (\nu^*)_{n+1}^{(z)};\ [(\bar{\sigma}_{ii})_1]_{n+1} = [(\bar{\sigma}_{ii})_1]_{n+1}^{(z)},\ (i = 1,2,3);$$

$$(\phi_1)_{n+1} = (\phi_1)_{n+1}^{(z)},\ (\phi_2)_{n+1} = (\phi_2)_{n+1}^{(z)};\quad \text{GOTO CN phase.}$$

Otherwise : SET $z = z + 1$; GOTO (b).

Fig. 2. (a) Algorithm for **ID** phase. (b) Algorithm for **CN** phase. (c) Algorithm for **CG** phase.

At the ID phase shown in Fig. 2(a), the converged value of Weibull probability function is calculated and the current volume fraction of fibers is updated. After computing the effective Young's moduli and Poisson's ratio at the end of ID phase using the updated value of fiber volume fraction, the program at the CN phase shown in Fig. 2(b) checks whether microcracks are nucleated by comparing current pressure with threshold pressure. If the microcracks are calculated to be nucleated, the number of microcracks is updated by using the Newton's method for the incremental form of crack nucleation. After computing the current stiffness tensor and its derivative with respect to current number of microcracks and updating the stresses, the program enters into the CG phase shown in Fig. 2(c) to compute the current value of mean crack radius.

(b)

(a) Initialize : $N_{n+1} = N_n,\ \boldsymbol{\epsilon}_{n+1} = \boldsymbol{\epsilon}_n + \Delta\boldsymbol{\epsilon}_{n+1}$

(b) Compute stiffness tensor : $\mathbf{C}_{n+1}$

(c) Compute increments : $(\Delta\boldsymbol{\sigma})_{n+1},\ (\Delta p)_{n+1}$

(d) Compute hydrostatic stress form of applied stress : σ_{n+1}

(e) Check whether cracks nucleate :

If $\sigma_{n+1} > \sigma_{no}$: then cracks nucleate

(1) Initialize : set $l = 0$; $N_{n+1}^{(0)} = N_n$ (for local Newton iteration)

(2) Solve nonlinear scalar equation for N_{n+1} (use local Newton iteration)

$$F[N_{n+1}^{(l)}] = N_{n+1}^{(l)} - N_n^{(l)} - \Delta t_{n+1}\dot{N}_o \cdot exp\left[\frac{(\sigma)_{n+1} - \sigma_{no}}{\sigma_1}\right]$$

(3) Perform convergence check :

If $\left|F[N_{n+1}^{(l)}]\right| \leq Tol\ (e.g., 10^{-8})$: set $N_{n+1} = N_{n+1}^{(l)}$; GOTO (4)

Otherwise set $l = l + 1$ and compute derivative of $F[N_{n+1}^{(l)}],\ dF[N_{n+1}^{(l)}]$

$$N_{n+1}^{(l+1)} = N_{n+1}^{(l)} - \frac{F[N_{n+1}^{(l)}]}{dF[N_{n+1}^{(l)}]}\ ;\ \text{GOTO (2)}$$

(4) Compute stiffness tensor : $\mathbf{C}_{n+1}$

(5) Compute derivative of $\mathbf{C}_{n+1}$ with respect to $N_{n+1},\ d\mathbf{C}[N_{n+1}]$

(6) Update stresses :

$$\boldsymbol{\sigma}_{n+1} = \boldsymbol{\sigma}_n + \mathbf{C} : \Delta\boldsymbol{\epsilon}_{n+1} + \frac{\partial\mathbf{C}}{\partial N}\Delta N_{n+1} : \boldsymbol{\epsilon}_n + \frac{\partial\mathbf{C}}{\partial N}\Delta N_{n+1} : \boldsymbol{\epsilon}_{n+1};\ \text{GOTO CG phase}$$

Otherwise : No crack nucleation. GOTO CG phase.

Fig. 2 (*continued*)

(c)

(a) Initialize : $\bar{c}_{n+1} = \bar{c}_n, \boldsymbol{\epsilon}_{n+1} = \boldsymbol{\epsilon}_n + \Delta\boldsymbol{\epsilon}_{n+1}$

(b) Compute stiffness tensor : $\mathbf{C}_{n+1}$

(c) Compute increments : $(\Delta\boldsymbol{\sigma})_{n+1},\ (\Delta p)_{n+1},\ (\Delta\mathbf{q})_{n+1}$

(d) Compute pressure and deviatoric stresses : $p_{n+1},\ q_{n+1}$

(e) Check whether material is within damage surface :

If $F(p_{n+1},\ q_{n+1}, \bar{c}_{n+1}) > 0$: then evolve crack radius

(1) Initialize : set $l = 0$; $\bar{c}^{(0)}_{n+1} = \bar{c}_n$ (for local Newton iteration)

(2) Solve nonlinear scalar equation for $\bar{c}_{n+1}$ (use local Newton iteration)

$$F[\bar{c}^{(l)}_{n+1}] = \bar{c}^{(l)}_{n+1} - \bar{c}^{(l)}_{n} - \beta\Delta t_{n+1}\sqrt{\frac{(E^*)^{(l)}_{n+1}}{\rho^*}}\tanh(d_s)$$

(3) Perform convergence check :

If $\left|F[\bar{c}^{(l)}_{n+1}]\right| \leq Tol\ (e.g., 10^{-8})$: set $\bar{c}_{n+1} = \bar{c}^{(l)}_{n+1}$; GOTO (4)

Otherwise set $l = l + 1$ and compute derivative of $F[\bar{c}^{(l)}_{n+1}],\ dF[\bar{c}^{(l)}_{n+1}]$

$$\bar{c}^{(l+1)}_{n+1} = \bar{c}^{(l)}_{n+1} - \frac{F[\bar{c}^{(l)}_{n+1}]}{dF[\bar{c}^{(l)}_{n+1}]};\ \text{GOTO (2)}$$

(4) Compute stiffness tensor : $\mathbf{C}_{n+1}$

(5) Compute derivative of $\mathbf{C}_{n+1}$ with respect to $\bar{c}_{n+1},\ d\mathbf{C}[\bar{c}_{n+1}]$

(6) Update stresses :

$$\boldsymbol{\sigma}_{n+1} = \boldsymbol{\sigma}_n + \mathbf{C} : \Delta\boldsymbol{\epsilon}_{n+1} + \frac{\partial\mathbf{C}}{\partial\bar{c}}\Delta\bar{c}_{n+1} : \boldsymbol{\epsilon}_n + \frac{\partial\mathbf{C}}{\partial\bar{c}}\Delta\bar{c}_{n+1} : \boldsymbol{\epsilon}_{n+1};\ \text{EXIT}$$

Otherwise : No crack growth; EXIT

Fig. 2 (*continued*)

The crack growth criteria presented in Eqs. (9) and (10) are applied to decide whether the size of microcracks increases at the current stress state. If the microcracks grow, the mean crack radius is iteratively computed by using the iterative Newton scheme for the nonlinear incremental Eq. (13). The stresses at the current load step are finally computed with the updated mean crack radius. It should be noted that the procedures described above are applied to each Gaussian integration point of all finite elements at each load increment step.

The numerical algorithms are based on the strain driven algorithm in which the stress history is to be determined by a given strain history. Therefore, the current computational approach could successfully deal with the softening behavior (negative stiffness zone). It is also worth mentioning that the current model can be easily extended to be able to model strain localization by relating potential fracture energy of the element size to the curve shape in the softening phase.

Two numerical examples are considered in this study. While the first example analyzes damage progression of composite plate coupon under dynamic loading, the second numerical example for drop tower test is simulated numerically to assess the potential of the implemented computational model for crashworthiness simulations.

4. Simulation of composite plate coupon test

A glass fiber polymeric composite plate under dynamic loading conditions is considered to observe the damage behavior of the composites. As shown in Fig. 3, the ratio of thickness, width, and length of the plate is assumed to be 1:10:100. Two loading conditions, compression and tension, are considered. The prescribed velocity $v(t)$ is imposed on the nodes on the top of the plate. The prescribed velocity is related to the rate of strain as

$$v(t) = \dot{\epsilon}L = \dot{\epsilon}L_0 \cdot \exp(\dot{\epsilon}t). \tag{17}$$

The prescribed velocity corresponding to $\dot{\epsilon} = 12/\mathrm{s}$ is applied in the direction as shown in Fig. 3 for compressive loading and in the opposite direction for tensile loading. The material properties of the composites used in this simulation are adopted from [23]: $E_{\mathrm{m}} = 3.0$ GPa, $v_{\mathrm{m}} = 0.35$, $E_{\mathrm{f}} = 72.0$ GPa, $v_{\mathrm{f}} = 0.17$, $\rho = 1403\ \mathrm{kg/m^3}$, $\phi_1 = 0.3$, $\alpha = 5.0$.

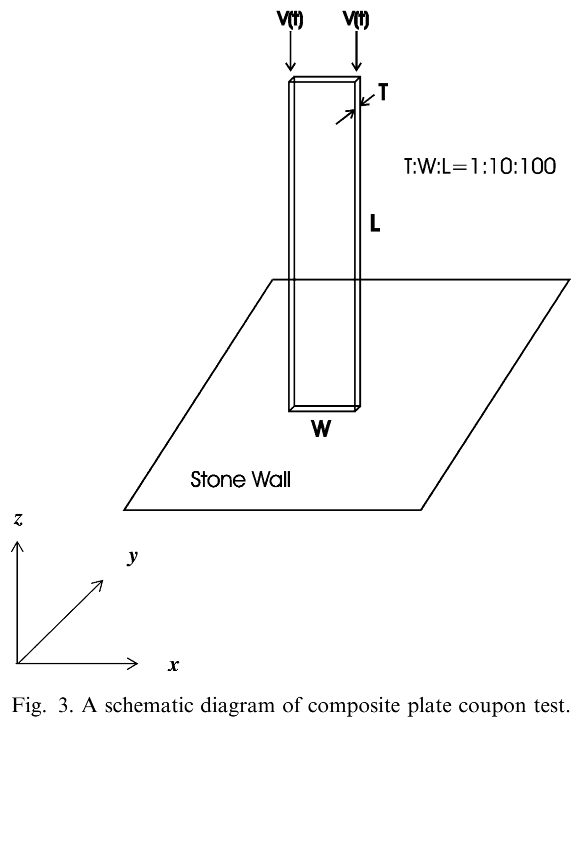

Fig. 3. A schematic diagram of composite plate coupon test.

The crack nucleation and growth related parameters, and Weibull parameters are assumed to be $\sigma_{n0} = 1.0 \times 10^{10}\ \mathrm{N/m^2}$, $\dot{N}_0 = 1.0 \times 10^{11}/\mathrm{s/m^3}$, $\sigma_1 = 2.0 \times 10^9\ \mathrm{N/m^2}$; $K_{\mathrm{IC}} = 10.0\ \mathrm{Pa\,m}$, $\beta = 1.0 \times 10^{-5}$, $\mu_0 = 0.26$, $N_0 = 1.0 \times 10^{11}/\mathrm{m^3}$, $\bar{c}_0 = 1.4 \times 10^{-5}$ m; $S_0 = 163.5$ MPa, and $M = 4.0$. These values are chosen from a combination of experimental results from the literature and do not correspond to a specific material.

Fig. 4 shows the stress–strain curves of the composite coupon under compression predicted by the crack nucleation (CN) damage model, crack growth (CG) damage model, and crack nucleation and growth (CNG) damage model. In the figure, each damage model predicts the softening behavior of the specimen after the peak load. CN model predicts the highest peak load with minimal evolution of damage, since the damage of the composite coupon is mainly due to the crack growth and the effect of crack nucleation on the degradation of specimen is negligible. It can be concluded that the substantial damage evolution occurs when the nucleated microcracks begin to grow or unstabilized since the damage parameter ω is much more strongly influenced by the size of microcracks than the number of microcracks ($\omega = N\bar{c}^3$).

Fig. 5 shows the predicted evolutions of the number of cracks versus strain and the mean crack radius versus strain corresponding to Fig. 4. It is

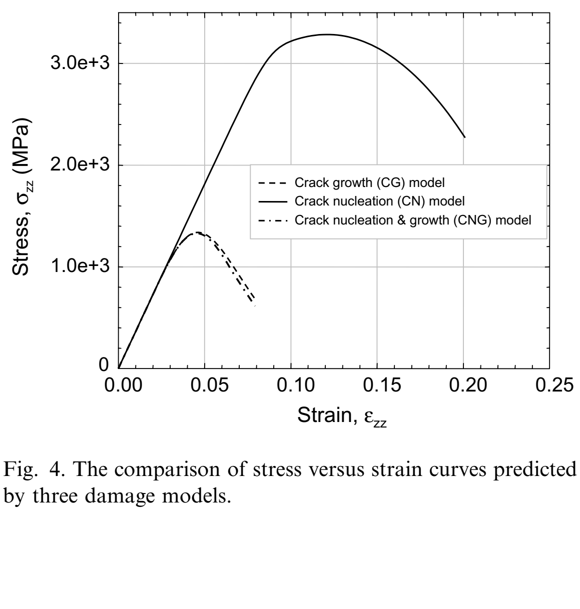

Fig. 4. The comparison of stress versus strain curves predicted by three damage models.

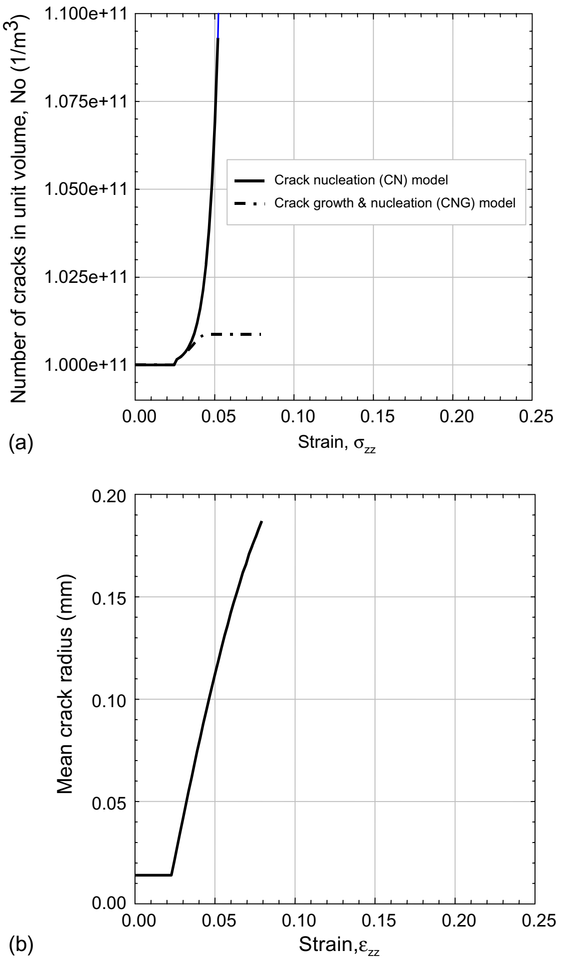

Fig. 5. The predicted evolutions of number of cracks versus strain (a) and crack size versus strain (b) corresponding to Fig. 4.

observed from Fig. 5(a) that the number of cracks remains constant at the initial stage of loading and then begins to increase at a certain threshold value of strain for both CN and CNG models. While the number of cracks N is increased only slightly and then remains constant again even at the deep strain range for the CNG model, it is increased very rapidly after the threshold strain in CN model. The value of strain at which the number of cracks begins to remain constant at the deep strain range of CNG model in Fig. 5 corresponds to the peak point of the stress–strain curve of CNG model in Fig. 4. Fig. 5(b) shows that the size of crack remains constant up to the threshold strain but, after that point, it suddenly begins to increase very rapidly until the compressed coupon reaches its ultimate strength in CG model. Finally, it is deduced for this particular example that, after the peak load, the number of cracks remain constant and the growth of crack dominates the softening behavior.

The damage behavior of the composite coupon shown in Fig. 3 under tensile loading with strain rate of $\dot{\epsilon} = 12$/s is analyzed by using the CG model and the combined interfacial fiber damage and crack growth (IDCG) damage model. Fig. 6 shows stress–strain curves of the composite coupon under tensile loading predicted by the two damage models. We observe from Fig. 6 that both models can predict the softening behavior induced by the damage mechanisms considered. The values of peak stresses for the tensile loading are found to be smaller than those for the compressive loading shown in Fig. 4. It is mainly because the existing cracks of the composite coupon under tensile loading begin to grow at a smaller value of strain as shown in Fig. 7. From Figs. 6 and 7, it can be seen that the interfacial fiber debonding affects both the stress–strain behavior and the evolution of crack growth of the coupon. Including the interfacial fiber debonding damage mechanism

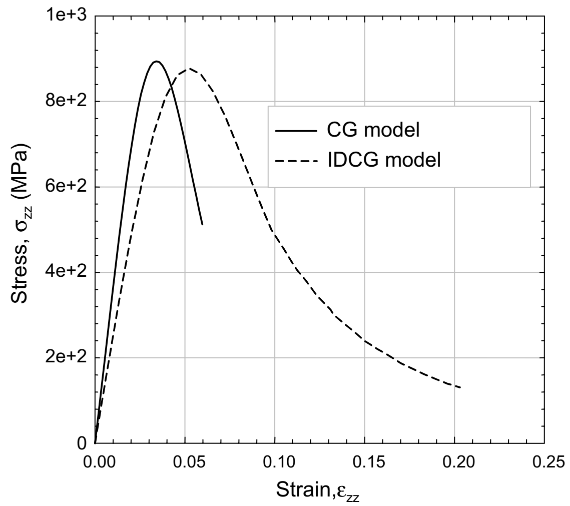

Fig. 6. The comparison between CG model and IDCG model for overall uniaxial, tensile responses of composites.

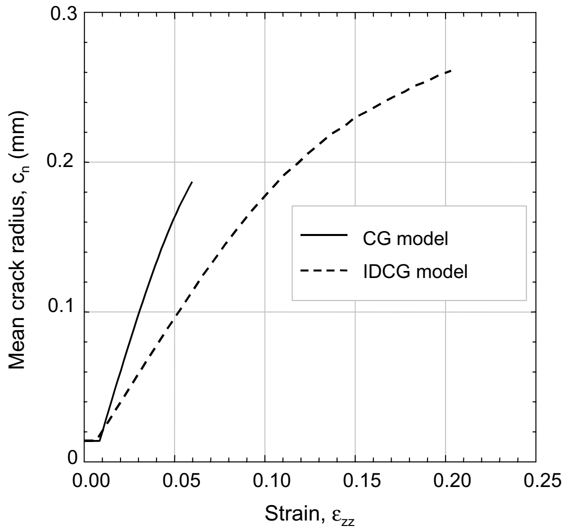

Fig. 7. The predicted evolution of crack size versus strain corresponding to Fig. 6.

into the crack growth damage model makes the composite coupon much more ductile with the peak stress remaining almost the same. It is also observed from Fig. 7 that the combined IDCG model predicts less steep rate of crack growth and greater size of crack at ultimate strength. Numerical results for the specimen under compressive and tensile loading show that the present approach is capable of modeling deterioration of effective stiffness of the composites and is stable in post-peak strain softening region.

The current model does not separately address the problem of localization of damage and failure. However, it turns out that the chopped random fiber materials possess particular failure event properties that alleviate this fundamental problem. In chopped random fiber materials, the localization and failure is shown to exhibit the characteristics of an uncorrelated one-dimensional event. Instead of breaking by the growth of a critical crack, the failure of the system is driven by the uncorrelated events (e.g., fiber breaks) in a one-dimensional zone that spans the system [3,10], which is orthogonal to the direction of the dominant strain. The width of the failure zone can be related to the fiber network characteristics and the size of the domain. Linear uncorrelated failure in a zone of finite width is compatible with the premises of the cohesive band framework [6], and the current model can be easily extended to include the cohesive band formulation. Alternatively, the localization can be handled by using the finite element resolution that corresponds to the characteristic size of failure localization features.

5. Simulation of crushing of drop tower

The drop tower test has been primarily used as a benchmark to evaluate the capabilities of energy absorption and to investigate crushing behavior of composite materials. A square, chopped carbon/polyurethane composite tube under impact loading is considered to simulate the damage evolution and crushing behavior of the composite tube. Since the crack growth mechanism is shown to dominate the damage behavior of the composites from the previous example, only the crack growth (CG) damage model is considered in this simulation. Fig. 8 shows the finite models for a drop mass, composite tube, and the initiator. In

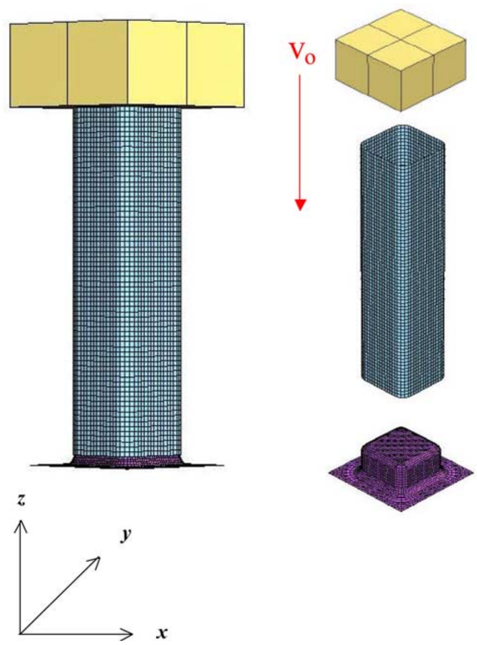

Fig. 8. Finite element model for drop tower simulation.

computational model, the drop mass is modeled by a single solid element and the composite tube is modeled by using Belyschko–Tsay shell elements. Nodes on the top edge of composite tube is tied to the bottom of solid element of drop mass. A contact surface is defined between the nodes of composite tube and segments of initiator element face. The initiator is modeled as rigid wall restrained in all degrees of freedom and laid at the bottom.

For the elements that lose their load-carrying capability as the cracks in the elements grow significantly, the element elimination algorithm provided in DYNA3D is applied to avoid numerical difficulties that may be encountered during numerical simulation. An initial velocity of 8.75 m/s is applied on nodes of composite tube and drop mass. The material properties of the carbon/polyurethane are $E_0 = 2.067$ GPa, $v_0 = 0.35$, $E_1 = 227.4$ GPa, $v_1 = 0.23$, $\rho = 1493$ kg/m^3, $\kappa^* = 213$ GPa, $\mu^* = 187$ GPa. We assumed the same fracture toughness K_{IC} and crack growth related parameters $\bar{c}_0$, N_0, μ_{fr}, β as those used in the previous example. In the user-material subroutines, history variables such as the volume fraction of damaged fibers, the number of microcracks, and the mean crack radius are monitored at each time step. It is assumed that the tube is reached to its ultimate failure either by the accumulation of growth of cracks (strain driven failure criterion) or by the excessive stresses (stress driven failure criterion).

Fig. 9 shows the sequence of deformed shaped of the square carbon/polyurethane composite tube. First, failure starts from the corner of composite tube. As the corner failure proceeds, the weakest segment of tube in the other direction is folded. The segment of folded section then fails. Fig. 10 shows the predicted force–displacement (P–u) curves for the composite tube. After P–u curves reach peak, they start to fluctuate due to progressive crushing of composite tube. Two failure criteria are employed in the drop tower test

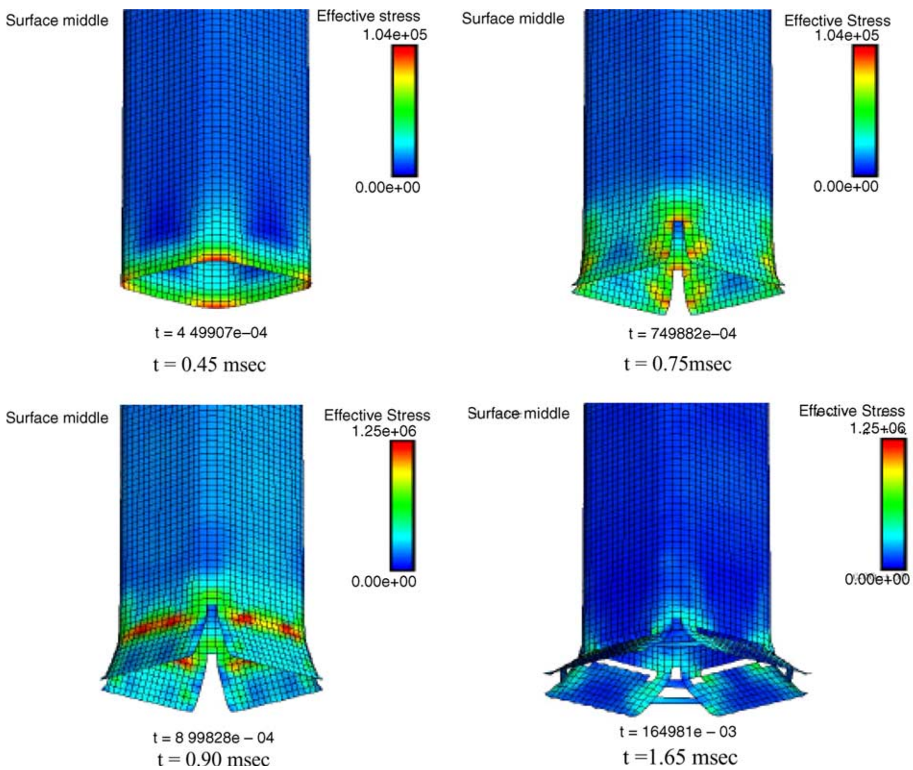

Fig. 9. A sequence of deformed shape of the square tube during crushing.

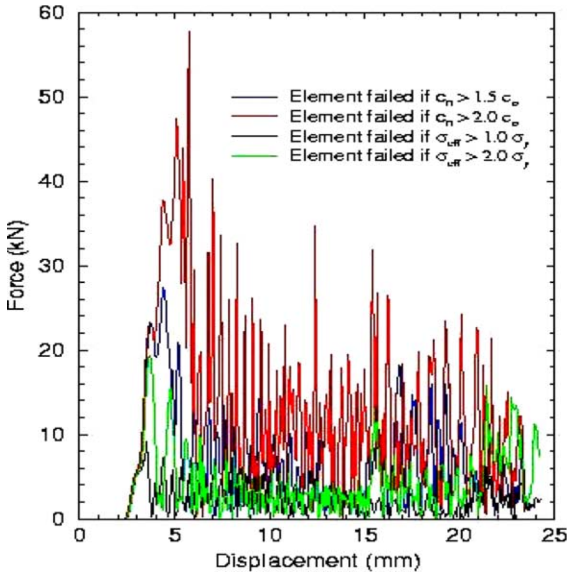

Fig. 10. The comparison of force–displacement (P–u) curves between two different failure criteria.

simulation: (1) stress driven failure criterion and (2) strain driven failure criterion. Fig. 11 exhibits a typical stress–strain curve of softened composites, where point A represents critical point of stress driven failure criterion and point B represents critical point of strain driven failure criterion. In

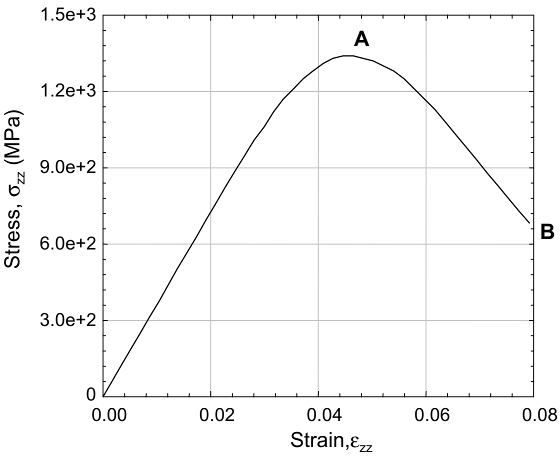

Fig. 11. Typical stress–strain curve of softened composites, where A and B represent critical points of stress driven and strain driven failure criteria, respectively.

Fig. 10, top two curves represent the predicted P–u curves for strain driven failure criterion. Because of the nature of two different failure criteria, one can observe that tube absorbs more energy when using a strain driven failure criterion.

6. Concluding remarks

The damage evolution of chopped random fiber composites under crushing type of loading was investigated. Material damages induced by the interfacial fiber debonding, the nucleation of microcracks, and the growth of cracks were considered. The systematic iterative computational algorithms were developed to combine the damage models in the constitutive relation. The user-supplied material subroutines were coded using the damage models and incorporated into the nonlinear finite element code DYNA3D. The capability of present computational damage approaches to model progressive deterioration of effective stiffness and softening behavior after the peak load was shown from benchmark examples on the composite coupon for compressive and tensile behavior.

The outcome from the numerical simulations on benchmark examples can be summarized as follows: (1) CG or CNG model would provide more accurate predictions of the damage constitutive behavior of the composites, since the effect of the crack growth on the constitutive behavior of the composites was shown to be more significant in comparison with the crack nucleation, and (2) the influence of the interfacial fiber debonding on the constitutive behavior of the composites was observed to be quite remarkable; therefore, IDCG model would be needed when simulating the composites having a weak interfacial bond strength. Crushing behavior of composite tube was also simulated, which shows the applicability of the proposed computational tool for crashworthiness simulations.

However, further investigations on responses of the composites under loading paths other than a uniaxial loading (e.g., shear, multiaxial state, cyclic loading, etc.) are needed to realistically assess the performance of the proposed computational algorithms and damage models. Numerical simulation for the crushing behavior of composite tube also shows the applicability of the present computational procedure for crashworthiness simulations. The developed damage model includes several model parameters that have to be input in the computer program. Future efforts need to be made to determine the parameters for the calibration of composite constitutive model. Furthermore, experimental crash tests for chopped random fiber composite structures are necessary to verify the present procedure on the crashworthiness simulations.

Acknowledgements

This research was sponsored by the US Department of Energy, Assistant Secretary for Energy Efficiency and Renewable Energy, Office of Transportation Technologies, Lightweight Materials Program, under contract DE-AC05-00OR22725 with UT-Battelle, LLC.

References

[1] F.L. Addessio, J.N. Johnson, A constitutive model for the dynamic response of brittle materials, J. Appl. Phys. 67 (1990) 3275–3286.

[2] P.F. Arndt, T. Nattermann, Criterion for crack formation in disordered materials, Phys. Rev. B (Condens. Matter Mater. Phys.) 63 (2001) 134204/1-8.

[3] J.A. Astrom, K.J. Niskanen, Symmetry-breaking fracture in random fibre networks, Europhys. Lett. 21 (1993) 557–562.

[4] D.R. Atodaria, S.K. Putatunda, P.K. Mallick, A fatigue crack growth model for random fiber composites, J. Compos. Mater. 31 (1997) 1838–1855.

[5] T.W. Barbee, L. Seaman, R.C. Crewdson, Dynamic fracture criteria of homogeneous materials, AFWL-TR-70-99, Air Force Weapons Laboratory, Albuquerque, NM, 1970.

[6] Z.P. Bazabt, Softening instability: Part I—localization into a planar band, J. Appl. Mech. 55 (1988) 517–522.

[7] G.P. Carman, K.L. Reifsnider, Micromechanics of short-fiber composites, Compos. Sci. Technol. 43 (1992) 137–146.

[8] C.H.J. Davies, Application of the renormalization group method to the failure of fibre bundles, J. Mater. Sci. Lett. 14 (1995) 1813–1814.

[9] D.R. Curran, D.A. Shockey, L. Seaman, Dynamic fracture criteria for a polycarbonate, J. Appl. Phys. 44 (1973) 4025–4038.

[10] A. Guarino, A. Garcimartin, S. Ciliberto, An experimental test of the critical behaviour of fracture precursors, Euro. Phys. J. B 6 (1998) 13–24.

[11] Z. Hashin, The differential scheme and its application to cracked materials, J. Mech. Phys. Solids 36 (1988) 719–734.

[12] H. Horii, A. Hasegawa, F. Nishino, Fracture process and bridging zone model and influencing factors in fracture of concrete, in: S.P. Shah, S.E. Swartz (Eds.), Fracture of Concrete and Rock, Springer-Verlag, New York, 1989, pp. 205–219.

[13] J.W. Ju, H.K. Lee, A Micromechanical damage model for effective elastoplastic behavior of ductile matrix composites considering evolutionary complete particle debonding, Comput. Methods Appl. Mech. Eng. 183 (2000) 201–222.

[14] B.L. Karihaloo, D. Fu, X. Huang, Modeling of tension softening in quasi-brittle materials by an array of circular holes with edge cracks, Mech. Mater. 11 (1991) 123–134.

[15] B.L. Karihaloo, X. Huang, Tensile response of quasi-brittle, PAGEOPH 137 (1991) 461–487.

[16] D. Krajcinovic, M. Vujosevic, Intrinsic failure modes of brittle materials, Int. J. Solids Struct. 35 (1998) 2487–2503.

[17] H.K. Lee, A computational approach to the investigation of impact damage evolution in discontinuously reinforced fiber composites, Comput. Mech. 27 (2001) 504–512.

[18] H.K. Lee, S. Simunovic, Modeling of progressive damage in aligned and randomly oriented discontinuous fiber polymer matrix composites, Compos. Part B: Eng. 31 (2000) 77–86.

[19] H.K. Lee, S. Simunovic, A damage constitutive model of progressive debonding in aligned discontinuous fiber composites, Int. J. Solids Struct. 38 (2001) 875–895.

[20] H.K. Lee, S. Simunovic, Prediction of crack evolution and stress–strain behavior of brittle materials, Comput. Struct., submitted for publication.

[21] A. Meddad, J. Azaiez, A. Ait-Kadi, Micromechanical modeling of tensile behavior of short fiber composites, J. Compos. Mater. 36 (2002).

[22] P.K. Mehta, P.J.M. Monteiro, Concrete: Structure, Properties, and Materials, Prentice-Hall, Englewood Cliffs, NJ, 1993.

[23] F. Meraghni, M.L. Benzeggagh, Micromechanical modeling of matrix degradation in randomly discontinuous-fibre composites, Compos. Sci. Technol. 55 (1995) 171–186.

[24] F. Meraghni, C.J. Blakeman, M.L. Benzeggagh, Effect of interfacial decohesion on stiffness reduction in a random discontinuous-fibre composite containing matrix microcracks, Compos. Sci. Technol. 56 (1996) 541–555.

[25] M. Ortiz, Microcrack coalescence and macroscopic crack growth initiation in brittle solids, Int. J. Solids Struct. 24 (1988) 231–250.

[26] L. Seaman, T.W. Barbee, D.R. Curran, Dynamic fracture criteria of homogeneous materials, AFWL-TR-71-156, Air Force Weapons Laboratory, Albuquerque, NM, 1971.

[27] L. Seaman, D.R. Curran, D.A. Shockey, Computational models for ductile and brittle fracture, J. Appl. Phys. 47 (1976) 4814–4826.

[28] D.A. Shockey, L. Seaman, D.R. Curran, Dynamic fracture of beryllium under plate impact and correlation with electron beam and underground test results, AFWL-TR-73-12, Air Force Weapons Laboratory, Albuquerque, NM, 1973.
[29] S. Sirivedin, D.N. Fenner, R.B. Nath, C. Galiotis, Matrix crack propagation criteria for model short-carbon fibre/epoxy composites, Compos. Sci. Technol. 60 (2000) 2835–2847.
[30] G.P. Tandon, G.J. Weng, Average stress in the matrix and effective moduli of randomly oriented composites, Compos. Sci. Technol. 27 (1986) 111–132.
[31] W. Wu, I. Verpoest, J. Varna, A novel axisymmetric variational analysis of stress transfer into fibres through a partially debonded interface, Compos. Sci. Technol. 58 (1998) 1863–1877.
[32] Y.H. Zhao, G.J. Weng, Plasticity of a two-phase composite with partially debonded inclusions, Int. J. Plast. 12 (1996) 781–804.
[33] Y.H. Zhao, G.J. Weng, Transversely isotropic moduli of two partially debonded composites, Int. J. Solids Struct. 34 (1997) 493–507.
[34] J.M. Duva, J. Aboudi, C.T. Herakovich, Probabilistic micromechanics model for damaged composites, J. Eng. Mater. Technol. 118 (1996) 548–553.